DOI:
10.1016/j.jorganchem.2018.07.005

Document Version
Peer reviewed version

Accepted Manuscript

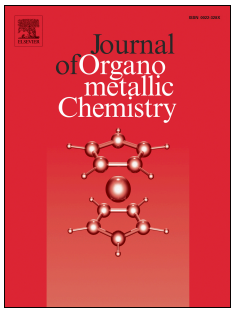

Diphosphine-induced thiolate-bridge scission of $[Re(CO)_3(\mu,\kappa^2\text{-S,N-thpymS})]_2$ (thpymS = 1,4,5,6-tetrahydropyrimidine-2-thiolate): Structural and computational studies of configurational isomers of $[Re(CO)_3(\kappa^2\text{-S,N-thpymS})]_2(\mu,\kappa^1,\kappa^1\text{-dppe})$

Md Rassel Moni, Shishir Ghosh, Shaikh M. Mobin, Derek A. Tocher, Graeme Hogarth, Michael G. Richmond, Shariff E. Kabir

PII: S0022-328X(18)30495-9

DOI: 10.1016/j.jorganchem.2018.07.005

Reference: JOM 20492

To appear in: *Journal of Organometallic Chemistry*

Received Date: 19 June 2018

Accepted Date: 6 July 2018

Please cite this article as: M.R. Moni, S. Ghosh, S.M. Mobin, D.A. Tocher, G. Hogarth, M.G. Richmond, S.E. Kabir, Diphosphine-induced thiolate-bridge scission of $[Re(CO)_3(\mu,\kappa^2\text{-S,N-thpymS})]_2$ (thpymS = 1,4,5,6-tetrahydropyrimidine-2-thiolate): Structural and computational studies of configurational isomers of $[Re(CO)_3(\kappa^2\text{-S,N-thpymS})]_2(\mu,\kappa^1,\kappa^1\text{-dppe})$, *Journal of Organometallic Chemistry* (2018), doi: 10.1016/j.jorganchem.2018.07.005.

Graphical Abstract

Diphosphine-induced thiolate-bridge scission of $[Re(CO)_3(\mu,\kappa^2\text{-S,N-thpymS})]_2$ (thpymS = 1,4,5,6-tetrahydropyrimidine-2-thiolate): Structural and computational studies of configurational isomers of $[Re(CO)_3(\kappa^2\text{-S,N-thpymS})]_2(\mu,\kappa^1,\kappa^1\text{-dppe})$

Md. Rassel Moni, Shishir Ghosh*, Shaikh M. Mobin, Derek A. Tocher, Graeme Hogarth, Michael G. Richmond, Shariff E. Kabir*

The reactions of binuclear $[Re(CO)_3(\mu,\kappa^2\text{-S,N-thpymS})]_2$ with diphosphines have been investigated which led to the isolation and characterization of a range of different products.

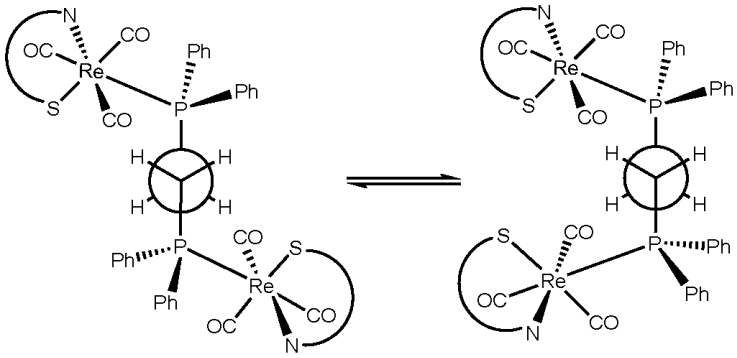

Diphosphine-induced thiolate-bridge scission of $[Re(CO)_3(\mu,\kappa^2\text{-S,N-thpymS})]_2$ (thpymS = 1,4,5,6-tetrahydropyrimidine-2-thiolate): Structural and computational studies of configurational isomers of $[Re(CO)_3(\kappa^2\text{-S,N-thpymS})]_2(\mu,\kappa^1,\kappa^1\text{-dppe})$

Md. Rassel Moni [a], Shishir Ghosh [a,*], Shaikh M. Mobin [b], Derek A. Tocher [c], Graeme Hogarth [d], Michael G. Richmond [e], Shariff E. Kabir [a,*]

[a] *Department of Chemistry, Jahangirnagar University, Savar, Dhaka 1342, Bangladesh*
[b] *Discipline of Chemistry, School of Basic Science, Indian Institute of Technology Indore, Khandwa Road, Indore 452 017, India*
[c] *Department of Chemistry, University College London, 20 Gordon Street, London, WC1H 0AJ, United Kingdom*
[d] *Department of Chemistry, King's College London, Britannia House, 7 Trinity Street, London SE1 1DB, UK*
[e] *Department of Chemistry, University of North Texas, Denton, TX 76209, USA*

*Corresponding Authors. Emails: sghosh_006@yahoo.com (S. Ghosh); skabir_ju@yahoo.com (S.E. Kabir)

ABSTRACT:

Reactions of binuclear $[Re(CO)_3(\mu,\kappa^2\text{-S,N-thpymS})]_2$ (**1**) with diphosphines have been investigated. At 298 K, dppm reacts to give mononuclear $[Re(CO)_3(\kappa^1\text{-dppm})(\kappa^2\text{-S,N-thpymS})]$ (**2**) through a phosphine-promoted scission of the dithiolate bridges that leaves one of the phosphine moieties free (dangling). Refluxing **2** in toluene leads to CO loss and formation of dinuclear $[Re_2(CO)_4(\mu\text{-dppm})(\mu,\kappa^2\text{-S,N-thpymS})_2]$ (**3**) whose rhenium centers are bridged by two thiolate groups and the dppm ligand. Treatment of **1** with dppe at room temperature furnishes $[Re(CO)_3(\kappa^2\text{-S,N-thpymS})]_2(\mu,\kappa^1,\kappa^1\text{-dppe})$ (**4**) where each phosphine center ligates the respective $d^6\text{-}ML_5$ rhenium fragment. Complex **4** exists as two distinct configurational isomers (**4a** and **4b**) that have been isolated and the solid-state structures characterized crystallographically. The principal difference in the stereoisomeric products is the orientation of the two $[Re(CO)_3(\kappa^2\text{- S,N-thpymS})]$ moieties at the anti-staggered Newman projection involving the P-C-C-P backbone of the dppe ligand. Both stereoisomers retain their identity in solution at ambient temperatures but equilibrate to a 1:1 mixture upon heating at 363 K for 1 h. The reaction of **1** with dppe in toluene at 383 K affords $[Re(CO)_2(\kappa^1\text{-dppe})_2(\kappa^2\text{-S,N-thpymS})]$ (**5**) containing two monodentate (dangling) diphosphine ligands. Thus, these seemingly simple reactions afford a

range of different products whose composition is highly dependent upon the experimental conditions employed and the nature of the diphosphine backbone. The reaction of **1** with dppe and the process responsible for the equilibration of the two configurational isomers of **4** have been investigated by electronic structure calculations.

Keywords: rhenium; diphosphines; tetrahydropyrimidine-2-thiolate; DFT

1. Introduction

Transition metal complexes containing heterocyclic thiolate ligands have attracted considerable attention as key constituents in metalloproteins [1-5] and as CVD and ALD precursors for electronic devices based on binary metal-sulfides employed in the semiconductor industry [6-9]. Many unique pharmacologically active drugs also exhibit a heterocyclic-based platform with an ancillary thiolate moiety [1, 10]. Heterocyclic thiolates are capable of coordinating metal compounds in a variety of ways, and the use of a coordinatively flexible thiolate ligand affords a wide range of structural motifs [11-20]. A long-term research theme within our laboratories has involved the reactivity investigation of transition metal carbonyls with heterocyclic thiols, and our results have revealed that the outcomes of these reactions are influenced by both the intrinsic reactivity of the metal carbonyl substrate and the structure of the initial heterocyclic thiol [21-42]. For example, reactions between $M_2(CO)_{10}$ (M = Mn, Re) and pyrimidine-2-thiol (pymSH) furnish tetranuclear "square-type" clusters $[M(CO)_3(\mu,\kappa^2\text{-S,N-pymS})]_4$ [28], while similar reactions with tetrahydropyrimidine-2-thiol (thpymSH) or pyridine-2-thiol (pySH) affords only dinuclear products $[M(CO)_3(\mu,\kappa^2\text{-S,N-thpymS})]_2$ [29, 34] and $[M(CO)_3(\mu,\kappa^2\text{-S,N-pyS})]_2$ [5, 22, 42], respectively. Further, structural analyses reveal that while $[M(CO)_3(\mu,\kappa^2\text{-S,N-thpymS})]_2$ adopt centrosymmetric structures, $[M(CO)_3(\mu,\kappa^2\text{-S,N-pyS})]_2$ adopt a chiral structure with C_2 symmetry in the solid state (Scheme 1). Moreover, the metal-sulfur (M–S) bond(s) are labile, making them highly versatile precursors of $[M(CO)_x(L)]$ (x = 2, 3; L = heterocyclic thiolate) fragments. For example, these thiolate-bridged dimers readily react with phosphines and amines (at room temperature) to afford a range of mononuclear complexes such as *fac*-$[M(CO)_3(\kappa^2\text{-L})(PR_3)]$, *cis*-$[M(CO)_2(\kappa^2\text{-L})(\kappa^2\text{-diphosphine})]$, *fac*-$[M(CO)_3(\kappa^2\text{-L})(\kappa^1\text{-diamine})]$, *cis*-$[M(CO)_2(\kappa^2\text{-L})(\kappa^1\text{-diphosphine})_2]$ [22-29]. Heating the thiolated-bridged dimers with other metal carbonyls affords mixed-metal complexes containing $[M(CO)_3(L)]$ fragments [30-36].

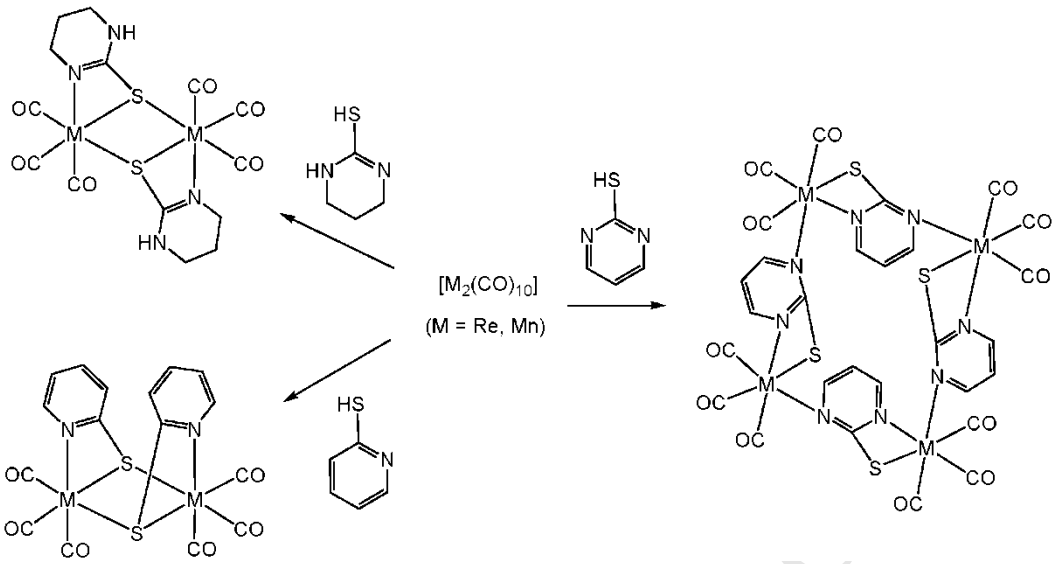

Scheme 1. Reactions of $[M_2(CO)_{10}]$ (M = Mn, Re) with pySH, pymSH and thpymSH.

In comparison to the extensive number of reports published for this genre of dinuclear complexes that adopt a chiral structure, very little attention has been paid to dinuclear complexes that adopt a centrosymmetric structure [29, 34]. In a continuation of our previous work, we now report on the reactivity of $[Re(CO)_3(\mu,\kappa^2\text{-S,N-thpymS})]_2$ (**1**) with the diphosphines, bis(diphenylphosphino)methane (dppm) and 1,2-bis(diphenylphosphino)ethane (dppe). Unexpectedly, the nature of the products generated is critically dependent on both the reaction conditions employed and the nature of the diphosphine used, and we present our results herein on the four different types of products that have been isolated and structurally characterized.

2. Experimental

2.1. General data

All the reactions were performed under a nitrogen atmosphere using standard Schlenk techniques. Reagent grade solvents were dried by standard procedures and freshly distilled prior to use. $Re_2(CO)_{10}$ (Strem) and tetrahydropyrimidine-2-thiol (thpymSH), dppm, and dppe (Acros Organics) were purchased and used as received. $[Re(CO)_3(\mu,\kappa^2\text{-S,N-thpymS})]_2$ was prepared according to the literature [29]. Products were separated without any special precautions on TLC plates coated with 0.25 mm silica gel (HF_{254}-type 60, E. Merck, Germany). IR spectra were recorded on a Shimadzu FTIR Prestige 21 spectrophotometer and

NMR spectra on a Varian Unity plus 500 spectrometer. All chemical shifts are reported in δ units and are referenced to the residual protons of the deuterated solvents (^{1}H) or to external H_3PO_4 (^{31}P), whose chemical shift is assigned to $\delta = 0.0$. Elemental analyses were performed by the Microanalytical laboratory of Wazed Miah Science Research Centre at Jahangirnagar University.

*2.2. Reaction of $[Re(CO)_3(\mu,\kappa^2\text{-}S,N\text{-}thpymS)]_2$ (**1**) with dppm*

A. Reaction at 298 K. To **1** (35 mg, 0.045 mmol) and dppm (35 mg, 0.091 mmol) under a nitrogen flow was added 15 mL of CH_2Cl_2. The solution was stirred at room temperature for 12 h, after which time the solvent was removed under reduced pressure and the residue purified by TLC. Elution with cyclohexane/CH_2Cl_2 (4:1, v/v) developed three bands. The first and third bands were identified as unreacted dppm (10 mg) and **1** (6 mg), respectively; the second band was confirmed as the desired product $[Re(CO)_3(\kappa^1\text{-dppm})(\kappa^2\text{-S,N-thpymS})]$ (**2**), which was isolated in 49% yield (34 mg) as colorless crystals after recrystallization from hexane/CH_2Cl_2 at 4 °C. Analytical and spectroscopic data for **2**: Anal. Calcd for $C_{32}H_{29}N_2O_3P_2ReS$: C, 49.93; H, 3.80; N, 3.64. Found: C, 50.67; H, 3.87; N, 3.69%. IR ($\nu_{co,}$ CH_2Cl_2): 2016 vs, 1915 s, 1886 s cm^{-1}. ^{1}H NMR ($CDCl_3$): δ 7.43 (m, 2H), 7.37 (m, 2H), 7.13 (m, 6H), 7.03 (m, 10H), 4.44 (s, 1H), 3.55 (m, 1H), 3.19 (m, 1H), 2.78 (m, 1H), 2.64 (m, 1H), 2.42 (m, 1H), 1.90 (m, 1H), 1.36 (m, 1H), 0.95 (m, 1H). ^{31}P{^{1}H} NMR ($CDCl_3$): δ 11.2 (d, 1P, J 75.0 Hz), -25.8 (d, 1P, J 75.0 Hz).

B. Reaction at 383 K. A toluene solution (15 mL) of **1** (50 mg, 0.065 mmol) and dppm (50 mg, 0.13 mmol) was stirred for 12 h at reflux. Upon cooling, the solvent was removed under reduced pressure and the residue chromatographed. Elution with cyclohexane/CH_2Cl_2 (7:3, v/v) developed four bands. The first and fourth bands were established by TLC analysis as unreacted dppm (8 mg) and **1** (trace), respectively. The second and third bands corresponded to $[Re(CO)_3(\kappa^1\text{-dppm})(\kappa^2\text{-S,N-thpymS})]$ (**2**) (8 mg, 8%) and the dinuclear compound $[Re_2(CO)_4(\mu\text{-dppm})(\mu,\kappa^2\text{-thpymS})_2]$ (**3**). The latter product was isolated in 38% yield (29 mg) as colorless crystals after recrystallization from hexane/CH_2Cl_2 at 4 °C. Analytical and spectroscopic data for **3**: Anal. Calcd for $C_{37}H_{36}N_4O_4P_2Re_2S_2\cdot CH_2Cl_2$: C, 38.54; H, 3.23; N, 4.73. Found: C, 39.17; H, 3.30; N, 4.77%. IR ($\nu_{co,}$ CH_2Cl_2): 1913 vs, 1834 s cm^{-1}. ^{1}H NMR ($CDCl_3$): δ 7.35 (m, 4H), 7.23-7.14 (m, 10H), 7.07 (m, 6H), 5.11 (s, 2H), 3.94 (t, 2H, J 10

Hz), 3.61 (m, 1H), 3.58 (m, 1H), 3.44 (m, 4H), 3.31 (m, 2H), 2.06 (m, 4H). $^{31}P\{^{1}H\}$ NMR ($CDCl_3$): δ 16.7 (s).

*2.3. Conversion of **2** to **3***

A toluene solution (10 mL) of **2** (30 mg, 0.039 mmol) was heated to reflux for 1 h. Upon cooling, the solvent was removed and the compounds **2** and **3** separated by TLC as described above. The first band was identified as **2** (9 mg) and the second band afforded **3**. The latter product was isolated in 56% (12 mg) as colorless crystals after recrystallization from hexane/CH_2Cl_2 at 4 °C.

*2.4. Reaction of $[Re(CO)_3(\mu,\kappa^2\text{-}S,N\text{-}thpymS)]_2$ (**1**) with dppe*

A. Room temperature reaction. To **1** (35 mg, 0.045 mmol) and dppe (36 mg, 0.090 mmol) was added 35 mL of CH_2Cl_2, and the solution was stirred at for 48 h. The solvent was removed under reduced pressure, and the residue was purified by TLC. Elution with cyclohexane/CH_2Cl_2 (7:3, v/v) gave four distinct bands with the first eluted band representing dppe (3 mg). The third and fourth bands were subsequently identified as the stereoisomers $[Re(CO)_3(\kappa^2\text{-}S,N\text{-}thpymS)]_2(\mu,\kappa^1,\kappa^1\text{-}dppe)]$ with **4a** eluting before **4b**. Both products were recrystallized from hexane/CH_2Cl_2 at 4ºC and afforded **4a** and **4b** as colorless crystals in 36% yield (22 mg) and 47 % yield (27 mg), respectively. The contents of the second band were too small for complete characterization and its identity was not pursued. Analytical and spectroscopic data for **4a**: Anal. Calcd for $C_{40}H_{38}N_4O_6P_2Re_2S_2\cdot 2CH_2Cl_2$: C, 37.67; H, 3.16; N, 4.18. Found: C, 38.21; H, 3.23; N, 4.22%. IR (ν_{CO}, CH_2Cl_2): 2016 vs, 1915 s, 1886 s cm^{-1}. ^{1}H NMR ($CDCl_3$): δ 7.47 (m, 3H), 7.40 (m, 2H), 7.34 (m, 9H), 7.25 (m, 5H), 4.47 (s, 2H), 2.87 (m, 4H), 2.70 (m, 2H), 2.42 (m, 4H), 1.91 (m, 2H), 1.43 (m, 2H), 0.84 (m, 2H). $^{31}P\{^{1}H\}$ NMR ($CDCl_3$): δ 14.8 (s). Analytical and spectroscopic data for **4b**: Anal. Calcd for $C_{40}H_{38}N_4O_6P_2Re_2S_2\cdot CH_2Cl_2$: C, 39.26; H, 3.22; N, 4.47. Found: C, 40.06; H, 3.29; N, 4.53%. IR (ν_{CO}, CH_2Cl_2): 2015 vs, 1914 s, 1884 s cm^{-1}. ^{1}H NMR ($CDCl_3$): δ 7.39-7.24 (m, 20H), 4.59 (s, 2H), 3.25 (t, 2H, J 15.0 Hz), 2.86 (m, 2H), 2.68 (m, 2H), 2.47 (m, 2H), 2.07 (m, 2H), 1.88 (m, 2H), 1.42 (m, 2H), 0.88 (m, 2H). $^{31}P\{^{1}H\}$ NMR ($CDCl_3$): δ 15.5 (s).

B. Reaction at 383 K. To a toluene solution (20 mL) of **1** (40 mg, 0.052 mmol) was added dppe (42 mg, 0.11 mmol), after which the reaction mixture was heated to reflux for 8 h. The solvent was removed under reduced pressure, and the residue chromatographed over silica

gel. Elution with cyclohexane/CH_2Cl_2 (3:2 v/v) developed four bands. The first and fourth bands were confirmed as dppe (12 mg) and **1** (7 mg), respectively. The second band afforded [$Re(CO)_2(\kappa^1$-dppe$)_2(\kappa^2$-thpymS)] (**5**) (36 mg, 30%) as colorless crystals after recrystallization from hexane/CH_2Cl_2 at 4 °C, while the amount of the third band was insufficient for thorough characterization. Analytical and spectroscopic data for **5**: Anal. Calcd for $C_{58}H_{55}N_2O_2P_4ReS$: C, 60.35; H, 4.80; N, 2.43. Found: C, 61.07; H, 4.88; N, 2.47%. IR ($\nu_{co,}$ CH_2Cl_2): 1920 vs, 1842 vs cm^{-1}. ^{1}H NMR($CDCl_3$): δ 7.91 (m, 3H), 7.85 (m, 4H), 7.63 (m, 2H), 7.51-7.22 (m, 31H), 4.38 (s, 1H), 3.03 (m, 2H), 2.81 (m, 2H), 2.60 (m, 2H), 2.40 (m, 2H), 2.23 (m, 2H), 1.71 (m, 2H), 1.21 (m, 2H). $^{31}P\{^1H\}$ NMR ($CDCl_3$): major isomer: δ 28.1 (d, J 8.0 Hz), 44.8 (d, J 8.0 Hz); minor isomer: δ 33.0 (d, J 4.0 Hz), 43.9 (d, J 4.0 Hz): major/minor = 2:1.

2.5. X-ray crystallography

Single crystals of **2**, **3**, **4a**, and **4b** suitable for X-ray diffraction analysis were grown by slow diffusion of hexane into a CH_2Cl_2 solution containing each compound. Suitable crystals were mounted on an Agilent Super Nova dual diffractometer (Agilent Technologies Inc., Santa Clara, CA) using a Nylon loop and Paratone oil and the diffraction data were collected at 150(2) K using Mo-Kα radiation (λ = 0.71073). Unit cell determination, data reduction, and absorption corrections were carried out using CrysAlisPro [43]. The structures were solved with the ShelXS [44] structure solution program by direct methods and refined by full-matrix least-squares on the basis of F^2 using ShelXL [44] within the OLEX2 [45] graphical user interface. Non-hydrogen atoms were refined anisotropically while the hydrogen atoms were included using a riding model. Pertinent crystallographic parameters are given in Table 1.

Place Table 1 Here

2.6. Computational details and modelling

The DFT calculations were carried out with the Gaussian 09 package of programs [46] using the B3LYP hybrid functional. This functional is comprised of Becke's three-parameter hybrid exchange functional (B3) [47] and the correlation functional of Lee, Yang, and Parr (LYP) [48]. Each rhenium atom was described with the Stuttgart-Dresden effective core potential and SDD basis set, [49] and the 6-31G(d') basis set [50] was employed for all remaining atoms. All reported geometries were fully optimized, and the analytical Hessian was evaluated at each stationary point to determine whether the geometry was an energy minimum (no negative eigenvalues) or a transition structure (one negative eigenvalue).

Unscaled vibrational frequencies were used to make zero-point and thermal corrections to the electronic energies, and the resulting enthalpies are reported in kcal/mol relative to the specified standard. Intrinsic reaction coordinate (IRC) calculations were performed on all transition-state structures in order to establish the reactant and product species associated with each transition-state structure. The geometry-optimized structures have been drawn with the *JIMP*2 molecular visualization and manipulation program [51].

3. Results and discussion

*3.1. Reaction of [Re(CO)$_3$(μ,κ^2-S,N-thpymS)]$_2$ (**1**) with dppm*

Earlier we reported that reaction of **1** with dppm at 80 °C gave mononuclear [Re(CO)$_3$(κ^1-dppm)(κ^2-S,N-thpymS)] (**2**) in 57% yield (Scheme 2) [29]. We have now conducted this reaction at two additional temperatures and found that the product distribution varies with temperature. At room temperature **2** is still generated, although the yield is lower because the reaction is slower, while in refluxing toluene the reaction also furnishes binuclear [Re$_2$(CO)$_4$(μ-dppm)(μ,κ^2-thpymS)$_2$] (**3**) as the major isolable product (38%). The higher temperature reaction was accompanied by extensive product decomposition as evidenced by the large amount of material that remains at the origin of the TLC plate. In a separate experiment, we showed that **2** transforms into **3** upon heating in refluxing toluene (Scheme 2).

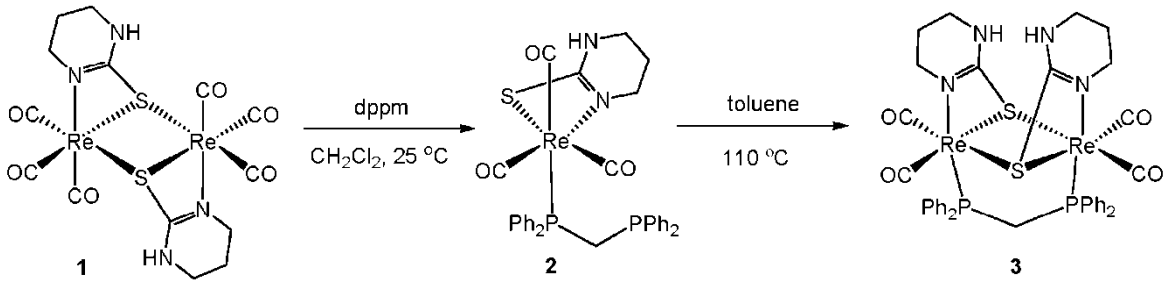

Scheme 2. Reaction of [Re(CO)$_3$(μ,κ^2-S,N-thpymS)]$_2$ (**1**) with dppm.

We have characterized both **2** (Fig. 1) and **3** (Fig. 2) by single-crystal X-ray diffraction. Selected bond distances and angles for **2** and **3** are given in the appropriate figure captions. Mononuclear **2** has a distorted octahedral geometry, and the coordination sphere about the rhenium reveals the presence of three facial carbonyls, an S,N-chelating tetrahydropyrimidine-2-thiolate ligand, and a monodentate (κ^1) diphosphine. The N–Re–S chelate angle of

66.67(17)° is similar to that observed in [Re(CO)$_3$(PPh$_3$)(κ^2-S,N-thpymS)] [64.05(9)°] [29]. Likewise, the Re–N [2.153(6) Å] and Re–P [2.4881(18) Å] bond distances are almost identical to those found in [Re(CO)$_3$(PPh$_3$)(κ^2-S,N-thpymS)], while the Re–S bond distance of 2.509(2) Å is *ca.* 0.05 Å shorter in the PPh$_3$-substituted derivative [29]. Binuclear **3** contains a dirhenium framework that is tethered by the dppm and two thpymS ligands. The S–Re–N chelate angles [S(2)–Re(1)–N(3) 64.68(10) and S(1)–Re(2)–N(1) 64.58(9)°] are similar to that in **2** and related thiolate-bridged complexes prepared by us [28-33, 37]. Each metal atom is also bound to two carbonyls which are positioned *trans* to the sulfur bridges. The starting complex **1** adopts a centrosymmetric structure where the tetrahydropyrimidine groups lie on opposite sides of the plane defined by the Re_2S_2 atoms, while in **3** the two heterocycles bridge the Re_2S_2 atoms that share a common side in order to create the proper environment for the dppm ligand to bridge the adjacent Re(1) and Re(2) atoms. The Re–P bond distances [Re(1)–P(1) 2.3412(10) and Re(2)–P(2) 2.3607(10) Å] are significantly shorter than that observed in **2** [2.4881(18) Å], while the Re–S bond distances [Re(1)–S(1) 2.5469(10), Re(1)–S(2) 2.5585(10), Re(2)–S(1) 2.5628(10), Re(2)–S(2) 2.5483(11) Å] are slightly longer than that found in **2** [2.509(2) Å]. The Re–N bond distances [Re(1)–N(3) 2.159(4) and Re(2)–N(1) 2.147(3) Å] in **3** are similar in length and are unremarkable with respect to related complexes [28-33, 37]. The spectroscopic data for **3** indicate that the solid-state structure persists in solution. The IR spectrum exhibits two strong carbonyl bands at 1913 and 1834 cm^{-1} while the $^{31}P\{^1H\}$ NMR spectrum shows a single resonance at δ 16.7 consistent with equivalent phosphorus atoms in the dppm ligand.

Place Figures 1 and 2 Here

Finally, we address the conversion of **2** → **3**. The exact sequence for this process is not known, but the product stoichiometry requires the formal loss of dppm from **2**. A rate-limiting dissociation of dppm from **2** would generate the unsaturated d^6-ML$_5$ species Re(CO)$_3$(κ^2-S,N-thpymS), which could be scavenged by the dangling phosphine group in unreacted **2** to give the dppm-bridged compound [*fac*-Re(CO)$_3$(κ^2-S,N-thpymS)]$_2$(μ,κ^1,κ^1-dppm). Loss of two CO groups, coupled with thiolate bridging of the adjacent rhenium centers, would afford **3**. That the capture of the dangling phosphine moiety in **2** is important en route to **3** was addressed by a control experiment. Heating **2** with **1** (0.5 equivalent) at 353 K gave **3** in high yield for those reactions that were monitored by TLC and IR spectroscopy.

*3.2. Reaction of [Re(CO)$_3$(μ,κ^2-S,N-thpymS)]$_2$ (**1**) with dppe*

Room temperature reaction of **1** and dppe (1:2 ratio) yields $[Re(CO)_3(\kappa^2\text{-thpymS})]_2(\mu,\kappa^1,\kappa^1\text{-dppe})$ (**4**) in 80 % yield by NMR. Analysis of the crude reaction mixture by TLC revealed the presence of two close running products in a 1:1 ratio, and the products were subsequently isolated and structurally characterized by X-ray crystallography. The right-hand portion of Scheme 3 illustrates this reaction.

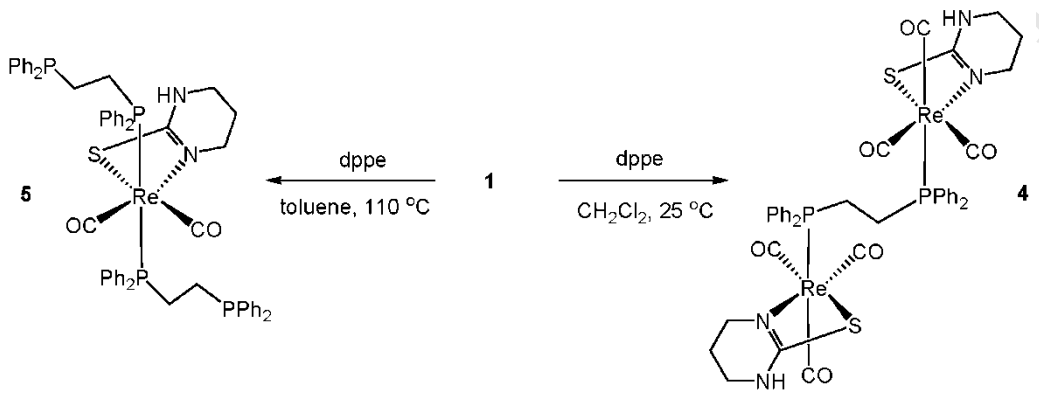

Scheme 3. Reactions of $[Re(CO)_3(\mu,\kappa^2\text{-S,N-thpymS})]_2$ (**1**) with dppe.

The solid-state structures for **4a** and **4b** are shown in Figs. 3 and 4, respectively, and the structures are confirmed as configurational stereoisomers. **4a** crystallizes in the monoclinic space group $P2_1/c$, and the asymmetric unit contains half of the molecule along with a molecule of CH_2Cl_2; **4b** crystallizes in the trigonal space group $P3_12_1$ and contains half a molecule of **4b** and CH_2Cl_2 in the asymmetric unit cell. Each structure of $[Re(CO)_3(\kappa^2\text{-S,N-thpymS})]_2(\mu,\kappa^1,\kappa^1\text{-dppe})$ contains a dppe ligand that coordinates two monomeric rhenium-tetrahydropyrimidine-2-thiolate subunits. The metric parameters displayed by **4a** and **4b** are very similar and within the range reported for related complexes [28-33, 37]. In both, the local geometry around each rhenium is best described as a distorted octahedron, and the bond angle found for each N–Re–S chelate is ca. 65°. An inversion center about the middle of the C(20)–C(20A) bond exists in **4a**, and this condition accounts for the coplanar environment and 180° torsion angle for the P(1)–C(20)–C(20A)–P(1A) atoms. Due to the absence of centrosymmetric symmetry in **4b**, the P(1)–C(20)–C(20A)–P(1A) torsion angle reveals a deviation from the ideal anti-periplanar orientation found in **4a** and exhibits with a slightly smaller torsion angle of 164.5°. Both products was also examined by DFT calculations, and the optimized structure of each product is shown alongside the experimentally determined structure. The structures computed for **4a** (**F**) and **4b** (**J**) exhibit excellent agreement with their respective solid-state structure.

Place Figures 3 and 4 Here

These stereoisomers are best viewed from the vantage of a Newman projection employing the P-C-C-P frame of the dppe ligand as the focal point for comparison of the differences displayed by the two $Re(CO)_3(\kappa^2$-S,N-thpymS) fragments in **4a** and **4b** (Scheme 4). The significant difference between the stereoisomers is the location of the $Re(CO)_3(\kappa^2$-S,N-thpymS) fragments about the Newman projections. The rhenium fragments adopt an anti-orientation in **4a** consistent with the symmetry-imposed inversion property, while in **4b** the two rhenium groups are located on the same side of the molecule. It should be noted that **4a** and **4b** are not rotamers and cannot interconvert via torsional rotation about any of the bonds in either species [52].

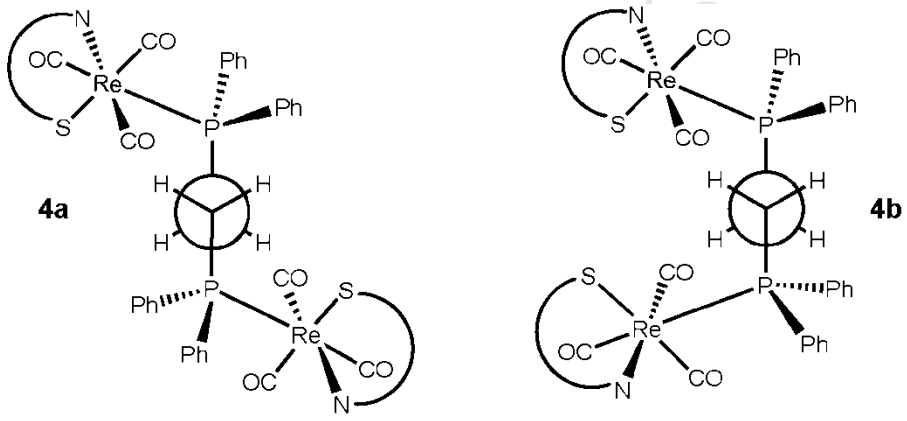

Scheme 4. Newman projections of **4a** (left) and **4b** (right) about the P-C-C-P frame of the dppe ligand.

Spectroscopic data confirm that **4a** and **4b** retain their identities in solution at ambient temperature under an inert atmosphere. The IR spectra show three characteristic carbonyl absorptions and the $^{31}P\{^1H\}$ NMR spectra show a distinct singlet for each stereoisomer (δ 14.8 for **4a** and δ 15.5 for **4b**). Compounds **4a** and **4b** are labile at elevated temperature, and heating each stereoisomer at 90 °C for 1 h readily generates an equimolar mixture containing **4a** and **4b** for those reactions monitored by ^{31}P NMR spectroscopy. The observation of a 1:1 mixture of stereoisomers after heating either **4a** or **4b** indicates a negligible energy difference between the two species and this feature, which was confirmed by DFT calculations, will be discussed in the next section.

In contrast to the products **4a** and **4b** produced from **1** and dppe at room temperature, thermolysis of **1** and dppe in refluxing toluene furnished $[Re(CO)_2(\kappa^1$-dppe$)_2(\kappa^2$-S,N-

thpymS)] (**5**) as the major product (30% yield). The nature of **5** is shown in Scheme 3 (left-hand portion), and the recorded spectroscopic data are in accord with the formulated structure. The IR spectrum shows two very strong carbonyl absorptions at 1920 and1842 cm^{-1} in excellent agreement with the frequencies reported by us for the pyridine-2-thiolate analog, $[Re(CO)_2(\kappa^1\text{-dppe})_2(\kappa^2\text{-S,N-pymS})]$ [28], which was prepared from the reaction of tetranuclear $[Re(CO)_3(\mu,\kappa^2\text{-S,N-pymS})]_4$ and dppe under similar conditions. The $^{31}P\{^1H\}$ NMR spectrum of **5** displays two sets of doublets in a 2:1 ratio that support the existence of a pair of isomers in solution. The set of resonances at δ 28.1 and 44.8 (J_{PP} 8 Hz) are attributed to the major isomer, while those at δ 33.0 and 43.9 (J_{PP} 4 Hz) are assigned to the minor isomer. The ^1H NMR spectrum is not particularly informative in terms of identifying the two isomers, but it does show resonances for the expected methylene protons of the dppe ligand and the heterocyclic residue, together with the NH moiety of the thpym group and the dppe aryl hydrogens.

3.3 Computational results

The reaction of **1** with dppe was investigated by electronic structure calculations in order to evaluate the energetic landscape leading to **4a** and **4b**. Dimer **1** is not unlike bromo-bridged $Br_2Re_2(CO)_6$ whose substitutional regioselectivity with ambidentate donors was recently examined [53]. This particular dimer reacts with incoming bidentate P-N donors as opposed to the unsaturated monomeric species $BrRe(CO)_4$ whose formation, relative to the reactant, is energetically prohibitive by 34.5 kcal/mol. Figs. 5 and 6 show the pertinent geometry-optimized structures and the energy surface en route to the products **F** and **J**. The dissociation of **1** to the unsaturated species $Re(CO)_3(\kappa^2\text{-S,N-thpym})$ (two equivalents) was evaluated, and the formation of **B** was computed to lie 32.6 kcal/mol above the reactant dimer. This energy difference is significant and allows us to exclude the participation of the monomeric species $Re(CO)_3(\kappa^2\text{-S,N-thpym})$ depicted in Scheme 5 in the reactions performed at room temperature. Species **A_alt**, which is 13.9 kcal/mol more stable than **B**, forms via the cleavage of one of the Re-S bonds in **A** to give an activated form of the starting dimer. The liberated rhenium center (black) in **A_alt** is five-coordinate and possesses a vacant site that can capture dppe to afford the mono-thiolate bridged species **D**. Disruption of a single thiolate bridge is accompanied by a penalty of 18.7 kcal/mol. The formation of the mono-substituted product $[Re(CO)_3(\kappa^1\text{-dppe})(\mu,\kappa^2\text{-S,N-thpymS})Re(CO)_3(\kappa^2\text{-S,N-thpymS})]$ (**D**) is exothermic by 9.8 kcal/mol and helps drive the reaction to products **F** and **J**. We also note

that the direct reaction of **A** and **C** to give **D** cannot be excluded from consideration at this juncture.

Place Figures 5 and 6 Here

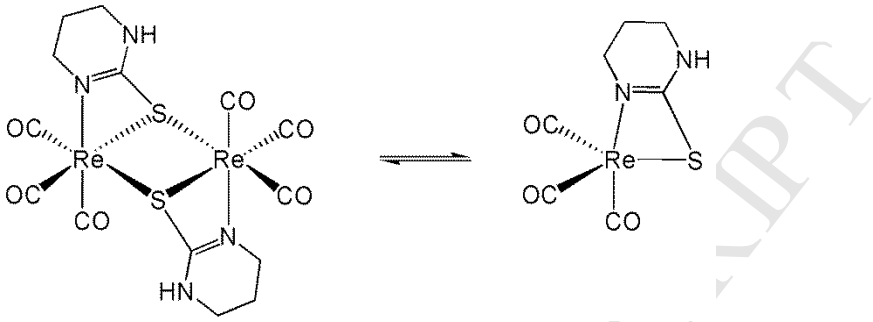

Scheme 5. $[Re(CO)_3(\mu,\kappa^2\text{-thpymS})]_2$ (**1**) dissociation to two equivalents of $Re(CO)_3(\kappa^2\text{-S,N-thpymS})$ monomer.

The conversion of **D** to **F** (as well as **J**) can, in theory, proceed through an intramolecular attack of the free phosphine moiety in **D** at the rhenium (red color; Fig. 5) that is bridged by the μ,κ^2-thpymS ligand. A concerted associative process that involves a saturated rhenium center lacks precedence based on the pioneering work of Atwood and Brown on related substitution reactions at six-coordinate Mn(I) and Re(I) derivatives [55], which, without exception, undergo ligand substitution through a dissociative manifold that furnishes a 16e d^6-ML_5 intermediate. The conversion of **D** → **E** and **B** is thus favored, and the sequence is completed by the capture of the dangling phosphine in **E** by the unsaturated species **B** to give **F** and **J**. The optimized structures of the two products are depicted alongside their X-ray diffraction structure in Figs. 3 and 4, respectively. Product **F** is 19.6 kcal/mol more stable than the reactants, and the energy difference (ΔH) between products **F** and **J** is small and favors the former by 0.7 kcal/mol.

We next address the equilibration of **4a** and **4b** observed on heating. As mentioned earlier, the equilibration process is symmetry prohibited and cannot proceed without bond breaking. Scheme 6 illustrates this using **4a** and utilizing the antiperiplanar conformation about the P-C-C-P frame to demonstrate the phenomenon. Rotation of the lower rhenium moiety in **4a** about the C-C-P-Re fold angle furnishes the depicted rotamer product. The dihedral rotation effectively translates the nitrogen heterocycle to a site syn to the unperturbed heterocycle associated with the upper rhenium unit. The spatial orientation of the two heterocycles in the rotameric product is different from the heterocycles in **4b**.

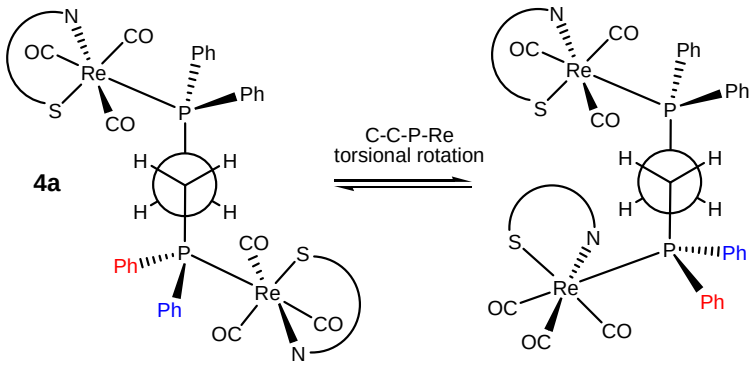

Scheme 6. Rotamer interconversion by rotation about the C-C-P-Re dihedral angle in **4a**.

Successful conversion of **F** → **J** was found to proceed by dissociative release of a coordinated nitrogen atom in one of the S,N-chelated rings. Fig. 7 shows the optimized structures and the energy surface appears in Fig. 8. The release of the coordinated nitrogen in **F** from the lower chelated heterocycle gives the trigonal-bipyramidal species **G** that contains an equatorial κ^1 thiolate moiety. **TSFG** serves as the rate-limiting step for the overall reaction, lying 26.8 kcal/mol above **F**. The unsaturated product **G** lies 1.9 kcal/mol below **TSFG**. The κ^1 thiolate group in **G** next undergoes a clockwise rotation by way of **TSGH** and where the forward motion of the heterocycle is coupled with chelate-ring closure to afford **H**. The final steps involve tandem C-C-P-Re torsional rotations that lead to the conversion of **H** → **I** → **J** and complete the formal equilibration of **F** → **J**.

Place Figures 7 and 8 Here

4. Summary and conclusions

Reaction between binuclear $[Re(CO)_3(\mu,\kappa^2\text{-thpymS})]_2$ (**1**) and dppm furnish mononuclear $[Re(CO)_3(\kappa^1\text{-dppm})(\kappa^2\text{-thpymS})]$ (**2**) at room temperature, while the same reaction conducted at elevated temperature in toluene affords dinuclear $[Re_2(CO)_4(\mu,\kappa^1,\kappa^1\text{-dppm})(\mu,\kappa^2\text{-thpymS})_2]$ (3) as the major product. Complex **2** contains a dangling dppm ligand, while the same diphosphine bridges two rhenium atoms in **3**. Normally the dinuclear framework of $[M(CO)_3(\mu\text{-L})]_2$ (M = Mn, Re; LH = heterocyclic thiol) type complexes breaks down during their reactions with phosphines due to the fragile nature of the M–S bond [5, 22-36]. Complex **3** is the second example in which the metal-sulfur bridges remain intact in the product, the other being $[Mn_2(CO)_5(PPh_3)(\mu,\kappa^2\text{-S,N-pyS})_2]$ which was synthesized from $[Mn_2(CO)_6(\mu,\kappa^2\text{-S,N-pyS})_2]$ at room temperature using $[(Ph_3P)_2Ni(CO)_2]$ as the phosphine

source [26]. Upon thermolysis in refluxing toluene, **2** transforms to **3** as demonstrated by independent control experiments. In contrast, a similar reaction between **1** and dppe at room temperature yields the configurational isomers $[Re(CO)_3(\kappa^2\text{-S,N-thpymS})]_2(\mu,\kappa^1,\kappa^1\text{-dppe})$ (**4a,b**) whose structures differ only by the orientation of $[Re(CO)_3(\kappa^2\text{-S,N-thpymS})]$ units about the P-C-C-P backbone of the dppe ligand. At ambient temperatures both **4a** and **4b** maintain their identity in solution, but they readily equilibrate to a 1:1 mixture at 90°C over a period of 1 h through a rate-limiting dissociation of one of the chelated nitrogen atoms in a thpymS ligand. In contrast, heating **1** and dppe in refluxing toluene gives only $[Re(CO)_2(\kappa^1\text{-dppe})_2(\kappa^2\text{-S,N-thpymS})]$ (**5**) which contains two dangling dppe ligands.

5. Acknowledgments

This research has been partly sponsored by the Ministry of Science and Technology, Bangladesh. MGR acknowledges financial support from the Robert A. Welch Foundation (Grant B-1093) and computational resources through CASCaM, which is supported by NSF (CHE-1531468).

6. Supplementary data

CCDC 1850357, CCDC 1850027, CCDC 1850363 and CCDC 1850034 contain supplementary crystallographic data for **2**, **3**, **4a** and **4b**, respectively. These data can be obtained free of charge via http://www.ccdc.cam.ac.uk/conts/retrieving.html, or from the Cambridge Crystallographic Data Centre, 12 Union Road, Cambridge CB2 1EZ, UK; fax: (+44) 1223-336-033; or e-mail: deposit@ccdc.cam.ac.uk. Atomic coordinates of all optimized structures are available from MGR on request.

References

[1] D. Katiyar, V.K. Tiwari, R.P. Tripathi, A. Srivastava, V. Chaturvedi, R. Srivastava, B.S. Srivastava, Bioorg. Med. Chem. 11 (2003) 4369.

[2] C.O. Kienitz, C. Thöne, P. Jones, Inorg. Chem. 35 (1996) 3990.

[3] R. Castro, M.L. Durán, J.A. Garcia-Vázquez, J. Romero, A. Sousa, A. Castiñeiras, W. Hiller, J. Strähle, J. Chem. Soc., Dalton Trans. (1990) 531.

[4] S.G. Rosenfield, H.P. Berends, L. Gelmini, D.W. Stephan, P.K. Mascharak, Inorg. Chem. 26 (1987) 2792.

[5] A.J. Deeming, M. Karim, P.A. Bates, M.B. Hursthouse, Polyhedron 7 (1988) 1401.

[6] J. Lee, T.J. Emge, J.G. Brennan, Inorg. Chem. 36 (1997) 5064.

[7] Y. Cheng, T.J. Emge, J.G. Brennan, Inorg. Chem. 35 (1996) 342.

[8] M. Berardini, J. Brennan, Inorg. Chem. 34 (1995) 6179.

[9] D.J. Rose, Y.D. Chang, Q. Chen, P.B. Kettler, J. Zubieta, Inorg. Chem. 34 (1995) 3973.

[10] K.H. Scheit, E. Gartner, Biochim. Biophys. Acta 183 (1969) 10.

[11] N. Choi, G. Conole, M. Kessler, J.D. King, M.J. Mays, M. McPartlin, G.E. Pateman, G.A. Solan, J. Chem. Soc. Dalton Trans. (1999) 3941.

[12] B. Cockerton, A.J. Deeming, M. Karim, K.I. Hardcastle, J. Chem. Soc., Dalton Trans. (1991) 431.

[13] A.J. Deeming, M. Karim, N.I. Powell, K.I. Hardcastle, Polyhedron 9 (1990) 623.

[14] A.J. Deeming, K.I. Hardcastle, M.N. Meah, P.A. Bates, H.M. Dawes, M.B. Hursthouse, J. Chem. Soc., Dalton Trans. (1988) 227.

[15] A.J. Deeming, M. Karim, N.I. Powell, J. Chem. Soc. Dalton Trans. (1990) 2321.

[16] N. Lugan, J.J. Bonnet, J.A. Ibers, J. Am. Chem. Soc. 107 (1985) 4484.

[17] B.F.G. Johnson, J. Lewis, D.A. Pippard, J. Chem. Soc. Dalton Trans. (1981) 407.

[18] S.G. Rosenfield, S.A. Swedberg, S.K. Arora, P.K. Mascharak, Inorg. Chem. 25 (1986) 2109.

[19] D.J. Rose, Y.D. Chang, Q. Chen, J. Zubieta, Inorg. Chem. 23 (1994) 5167.

[20] S. Kitagawa, M. Munakata, H. Shimono, S. Matsuyama, S. Masuda, J. Chem. Soc. Dalton Trans. (1990) 2105.

[21] S.E. Kabir, G. Hogarth, Coord. Chem. Rev. 253 (2009) 1285.

[22] S.E. Kabir, M.M. Karim, K. Kundu, S.M.B. Ullah, K.I. Hardcastle, J. Organomet. Chem. 517 (1996) 155.

[23] M. Islam, C.A. Johns, S.E. Kabir, K. Kundu, K.M.A. Malik, S.M.B. Ullah, J. Chem. Crystallogr. 29 (1999) 1001.

[24] M. Islam, S.E. Kabir, K. Kundu, K.M.A. Malik, S.M.B. Ullah, J. Chem. Crystallogr. 30 (2000) 379.

[25] G. Ara, S.E. Kabir, K. Kundu, K.M.A. Malik, J. Chem. Crystallogr. 33 (2003) 851.

[26] M.S. Rahman, J.C. Sarker, S. Ghosh, S.E. Kabir, Aus. J. Chem. 65 (2012) 796.

[27] S.E. Kabir, F. Ahmed, S. Ghosh, R.A. Mamun, D.T. Haworth, S.V. Lindeman, T.A. Siddiquee, D.W. Bennett, J. Chem. Crystallogr. 39 (2009) 595.

[28] S.E. Kabir, J. Alam, S. Ghosh, K. Kundu, G. Hogarth, D.A. Tocher, G.M.G. Hossain, H.W. Roesky, Dalton Trans. (2009) 4458.

[29] M.F. Ahmad, J.C. Sarker, K.A. Azam, S.E. Kabir, S. Ghosh, G. Hogarth, T.A. Siddiquee, M.G. Richmond, J. Organomet. Chem. 728 (2013) 30.

[30] S. Ghosh, S.E. Kabir, S. Pervin, G.M.G. Hossain, D.T. Haworth, S.V. Lindeman, T.A. Siddiquee, D.W. Bennett, H.W. Roesky, Z. Anorg, Allg. Chem. 635 (2009) 76.

[31] S. Ghosh, S.E. Kabir, S. Pervin, A.K. Raha, G.M.G. Hossain, D.T. Haworth, S.V. Lindeman, D.W. Bennett, T.A. Siddiquee, L. Salassa, H.W. Roesky, J. Chem. Soc. Dalton Trans. (2009) 3510.

[32] S. Ghosh, K.N. Khanam, G.M.G. Hossain, D.T. Haworth, S.V. Lindeman, G. Hogarth, S.E. Kabir, New J. Chem. 34 (2010) 1875.

[33] S. Ghosh, K.N. Khanam, M.K. Hossain, G.M.G. Hossain, D.T. Haworth, S.V. Lindeman, G. Hogarth, S.E. Kabir, J. Organomet. Chem. 695 (2010) 1146.

[34] S. Ghosh, F.K. Camellia, K. Fatema, M.I. Hossain, M.R. Al-Mamum, G.M.G. Hossain, G. Hogarth, S.E. Kabir, J. Organomet. Chem. 696 (2011) 2935.

[35] A.K. Raha, S. Ghosh, I. Hossain, S.E. Kabir, B.K. Nicholson, G. Hogarth, L. Salassa, J. Organomet. Chem. 696 (2011) 2153.

[36] S. Ghosh, M.S.A. Mia, E. Begum, G.M.G. Hossain, S.E. Kabir, Inorg. Chim. Acta 384 (2012) 76.

[37] A. Hoque, S. Islam, M. Karim, S. Ghosh, G. Hogarth, Inorg. Chem. Commun. 54 (2015) 69.

[38] M.R. Haque, S. Ghosh, G. Hogarth, M.G. Richmond, S.E. Kabir, Inorg. Chim. Acta 434 (2015) 150-157.

[39] M.A.H. Chowdhury, S. Rajbangshi, M. Karim, S. Ghosh, S.E. Kabir, T.A. Siddiquee, V.N. Nesterov, M.G. Richmond, Inorg. Chim. Acta 434 (2015) 97.

[40] S. Ghosh, S.E. Kabir, M. Khatun, D.T. Haworth, S.V. Lindeman, T.A. Siddiquee, D.W. Bennett, J. Chem. Crystallogr. 39 (2009) 632.

[41] M.A. Khaleque, K.A. Azam, M.M. Karim, S. Ghosh, G. Hogarth, S.E. Kabir, Aus. J. Chem. 65 (2012) 773.

[42] S.E. Kabir, S. Ghosh, N. Begum, G.M.G. Hossain, J. Bangladesh Chem. Soc. 22 (2009) 66.

[43] CrysAlisPro; Oxford Diffraction: Yarnton, England, 2015.

[44] G.M. Sheldrick, Acta Crystallogr., Sect. A: Found. Crystallogr. 64 (2008) 112-122.

[45] O.V. Dolomanov, L.J. Bourhis, R.J. Gildea, J.aK. Howard, H. Puschmann, J. Appl. Crystallogr. 42 (2009) 339-341.

[46] M.J. Frisch, G.W. Trucks, H.B. Schlegel, G.E. Scuseria, M.A. Robb, J.R. Cheeseman, G. Scalmani, V. Barone, B. Mennucci, G.A. Petersson, H. Nakatsuji, M. Caricato, X. Li, H.P. Hratchian, A.F. Izmaylov, J. Bloino, G. Zheng, J.L. Sonnenberg, M. Hada, M. Ehara, K. Toyota, R. Fukuda, J. Hasegawa, M. Ishida, T. Nakajima, Y. Honda, O. Kitao, H. Nakai, T. Vreven, J.A. Montgomery, Jr., J.E. Peralta, F. Ogliaro, M. Bearpark, J.J.. Heyd, E. Brothers, K.N. Kudin, V. N. Staroverov, R. Kobayashi, J. Normand, K. Raghavachari, A. Rendell, J.C. Burant, S.S. Iyengar, J. Tomasi, M. Cossi, N. Rega, J.M. Millam, M. Klene, J.E. Knox, J.B. Cross, V. Bakken, C. Adamo, J. Jaramillo, R. Gomperts, R.E. Stratmann, O. Yazyev, A.J. Austin, R. Cammi, C. Pomelli, J.W. Ochterski, R.L. Martin, K. Morokuma, V.G. Zakrzewski, G.A. Voth, P. Salvador, J.J. Dannenberg, S. Dapprich, A.D. Daniels, O. Farkas, J.B. Foresman, J.V. Ortiz, J. Cioslowski, D.J. Fox, Gaussian 09, Revision A.02, Gaussian, Inc., Wallingford CT, 2009.

[47] A.D. Becke, J. Chem. Phys. 98 (1993) 5648.

[48] C. Lee, W. Yang, R.G. Parr, Phys. Rev. B 37 (1988), 785.

[49] D. Andrae, U. Haeussermann, M. Dolg, H. Stoll, H. Preuss, Theor. Chem. Acc. 77 (1990) 123.

[50] (a) G.A. Petersson, A. Bennett, T.G. Tensfeldt, M.A. Al-Laham, W.A. Shirley, J. Mantzaris, J. Chem. Phys. 89 (1988) 2193. (b) G.A. Petersson, M.A. Al-Laham, J. Chem. Phys. 94 (1991) 6081.

[51] (a) JIMP2, version 0.091, a free program for the visualization and manipulation of molecules: M.B. Hall, R.F. Fenske, Inorg. Chem. 11 (1972) 768. (b) J. Manson, C.E. Webster, M.B. Hall, Texas A&M University, College Station, TX, 2006: http://www.chem.tamu.edu/jimp2/index.html.

[52] (a) Torsional rotation about any of the single bonds in **4a** or **4b** does not furnish its experimental counterpart. As such, the terms conformational isomer and rotamer are inaccurate descriptors for **4a** and **4b** since these terms can only be applied to those isomeric compounds that are interconvertible by free rotation about the bonds in the molecule. (b) J. March, "Advanced Organic Chemistry," 4th edition, Wiley, New York, 1992.

[53] D.D. Mayberry, V.N. Nesterov, M.G. Richmond, Eur. J. Inorg. Chem. (2017) 3990.

[54] J.D. Atwood, T.L. Brown, J. Am. Chem. Soc. 97 (1975) 3380; 98 (1976) 3155; 98 (1976) 3160.

Table 1. Crystal data and structure refinement details for compounds **2**, **3**, **4a**, and **4b**

Compound	**2**	**3**	**4a**	**4b**
Empirical formula	$C_{32}H_{29}N_2O_3P_2ReS$	$2(C_{37}H_{36}N_4O_4P_2Re_2S_2 \cdot CH_2Cl_2)$	$C_{21}H_{22}Cl_2N_2O_3PReS$	$C_{20.5}H_{19}ClN_2O_3PReS$
Formula weight	769.77	2368.16	670.54	626.06
Temperature (K)	150(2)	150(1)	150(2)	150.0(1)
Wavelength (Å)	0.71073	0.71073	0.71073	0.71073
Crystal system	monoclinic	triclinic	monoclinic	trigonal
Space group	$P2_1/c$	$P\text{-}1$	$P2_1/c$	$P3_12_1$
Unit cell dimensions				
a (Å)	14.559(5)	9.6219(2)	9.484(5)	11.0497(2)
b (Å)	12.327(5)	11.7899(3)	18.754(5)	11.0497(2)
c (Å)	18.478(5)	19.8646(5)	14.141(5)	31.4849(6)
α (°)	90	94.131(2)	90	90
β (°)	109.100(5)	103.241(2)	91.928(5)	90
γ (°)	90	105.388(2)	90	120
Volume (Å^3)	3133.7(19)	2093.63(10)	2513.7(17)	3329.14(14)
Z	4	1	4	6
Density (calculated) (Mg/m^3)	1.632	1.878	1.772	1.874
Absorption coefficient (mm^{-1})	4.081	6.124	5.218	5.786
F(000)	1520	1144	1304	1818
Crystal size (mm^3)	0.33 × 0.26 × 0.21	0.30 × 0.12 × 0.04	0.33 × 0.26 × 0.21	0.30 × 0.22 × 0.20
Θ range for data collection (°)	1.48 to 26.071	2.747 to 29.508	3.06 to 25	2.881 to 29.466
Index ranges	$-16 \le h \le 17$, $-14 \le k \le 15$, $-20 \le l \le 22$	$-12 \le h \le 13$, $-16 \le k \le 15$, $-26 \le l \le 26$	$-11 \le h \le 11$, $-22 \le k \le 22$, $-16 \le l \le 14$	$-13 \le h \le 14$, $-14 \le k \le 14$, $-42 \le l \le 40$
Reflections collected	22128	36179	19498	55629
Independent reflections [R_{int}]	6134 [R_{int} = 0.0221]	10320 [R_{int} = 0.0421]	4422 [R_{int} = 0.0349]	5836 [R_{int} = 0.0634]
Data / restraints / parameters	6134 / 1 / 374	10320 / 0 / 497	4422 / 0 / 280	5836 / 0 / 280
Goodness of fit on F^2	1.110	0.780	1.061	1.139
Final R indices [$I > 2\sigma(I)$]	R_1 = 0.0511, wR_2 = 0.1300	R_1 = 0.0293, wR_2 = 0.0936	R_1 = 0.0299, wR_2 = 0.0752	R_1 = 0.0261, wR_2 = 0.0465
R indices (all data)	R_1 = 0.525, wR_2 = 0.1308	R_1 = 0.0366, wR_2 = 0.1050	R_1 = 0.0354, wR_2 = 0.0797	R_1 = 0.0278, wR_2 = 0.0473
Largest diff. peak and hole (e. Å^{-3})	3.71 and –2.23	2.41 and –1.71	1.40 and –1.06	1.07 and –1.34

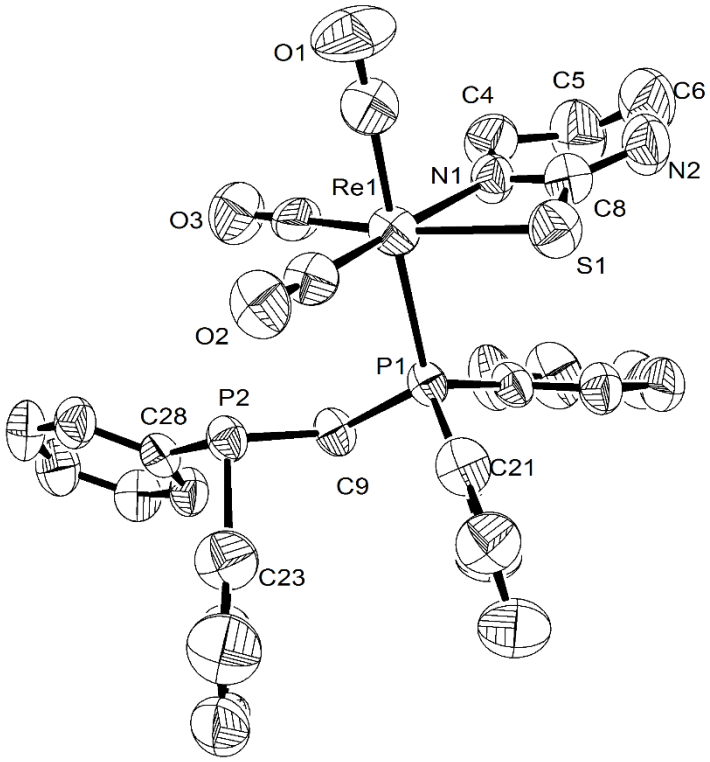

Fig. 1. Solid-state molecular structure of [Re(CO)$_3$(κ^1-dppm)(κ^2-S,N-thpymS)] (**2**) showing 50% thermal ellipsoids. Hydrogen atoms are omitted for clarity. Selected bond lengths [Å] and bond angles [°]: Re(1)–N(1) 2.153(6), Re(1)–P(1) 2.4881(18), Re(1)–S(1) 2.509(2), Re(1)–C(1) 1.947(9), Re(1)–C(2) 1.932(8), Re(1)–C(3) 1.969(8), N(1)–Re(1)–P(1) 88.98(18), N(1)–Re(1)–S(1) 66.67(17), P(1)–Re(1)–S(1) 87.52(7), N(1)–Re(1)–C(3) 94.2(4), N(1)–Re(1)–C(2) 172.9(3), S(1)–Re(1)–C(2) 106.5(2), S(1)–Re(1)–C(3) 160.8(3), P(1)–Re(1)–C(2) 92.6(2), P(1)–Re(1)–C(1) 178.5(3), P(1)–C(9)–P(2) 115.5(3).

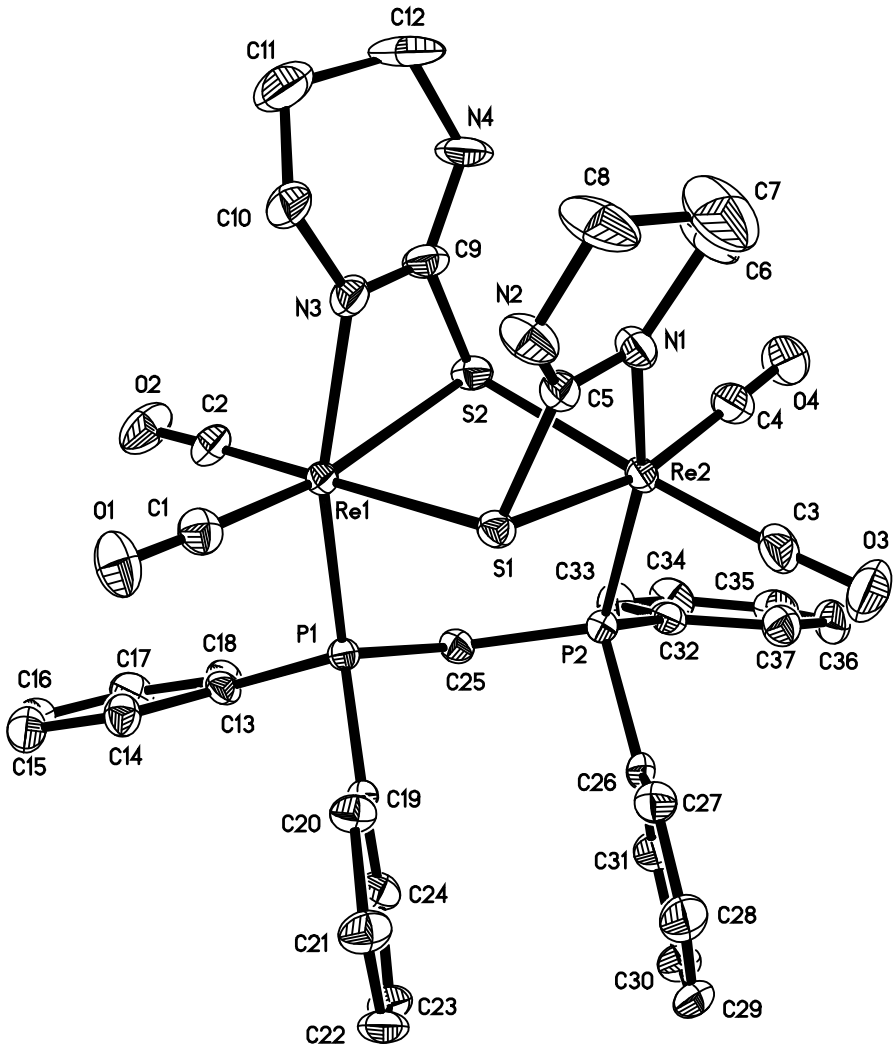

Fig. 2. Solid-state molecular structure of $[Re_2(CO)_4(\mu,\kappa^1,\kappa^1\text{-dppm})(\mu,\kappa^2\text{-S,N-thpymS})_2]$ (**3**) showing 50% thermal ellipsoids. Hydrogen atoms are omitted for clarity. Selected bond lengths [Å] and bond angles [°]: Re(1)–P(1) 2.3412(10), Re(2)–P(2) 2.3607(10), Re(1)–N(3) 2.159(4), Re(2)–N(1) 2.147(3), Re(1)–S(1) 2.5469(10), Re(1)–S(2) 2.5585(10), Re(2)–S(1) 2.5628(10), Re(2)–S(2) 2.5483(11), Re(1)–C(1) 1.878(5), Re(1)–C(2) 1.883(4), Re(2)–C(3) 1.882(5), Re(2)–C(3) 1.881(5), Re(1)–S(1)–Re(2) 92.82(3), Re(1)–S(1)–Re(2) 92.89(3), S(1)–Re(1)–S(2) 84.62(3), S(1)–Re(2)–S(2) 84.51(3), S(2)–Re(1)–N(3) 64.68(10), S(1)–Re(2)–N(1) 64.58(9), N(3)–Re(1)–C(1) 103.88(17), N(3)–Re(1)–C(2) 94.94(16), C(1)–Re(1)–C(2) 89.24(19), P(1)–Re(1)–N(3) 161.45(10), S(1)–Re(1)–N(3) 86.26(10), P(1)–Re(1)–S(1) 90.21(3), P(1)–C(25)–P(2) 117.8(2).

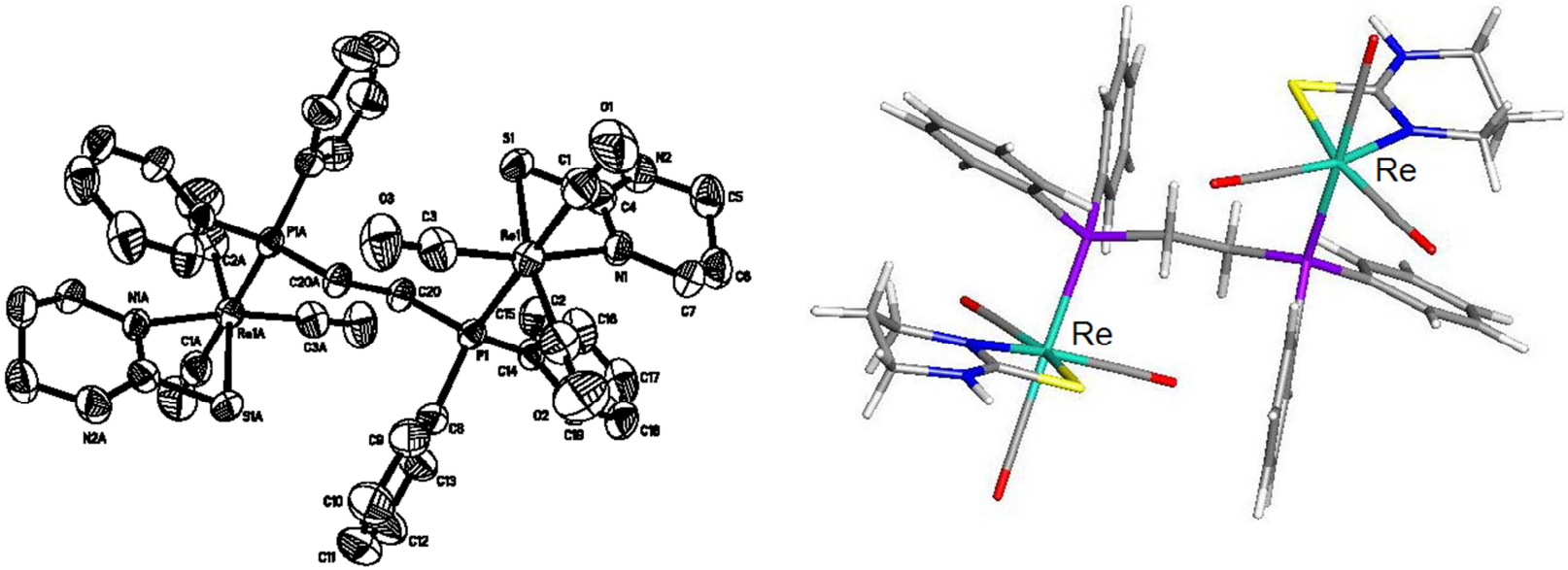

Fig. 3. Thermal ellipsoid plot of the molecular structure of **4a** (left) and the DFT-optimized structure of **F** (right). Thermal ellipsoids are displayed at 50% probability. Selected bond lengths [Å] and bond angles [°] from the X-ray diffraction structure: Re(1)–P(1) 2.4764(1), Re(1)–N(1) 2.164(4), Re(1)–S(1) 2.5465(2), P(1)–C(20) 1.842(5), C(20)–C(20A) 1.532(9), N(1)–Re(1)–S(1) 64.80(1), N(1)–Re(1)–P(1) 88.48(1), C(1)–Re(1)–S(1) 91.81(2), C(1)–Re(1)–C(2) 91.0(3).

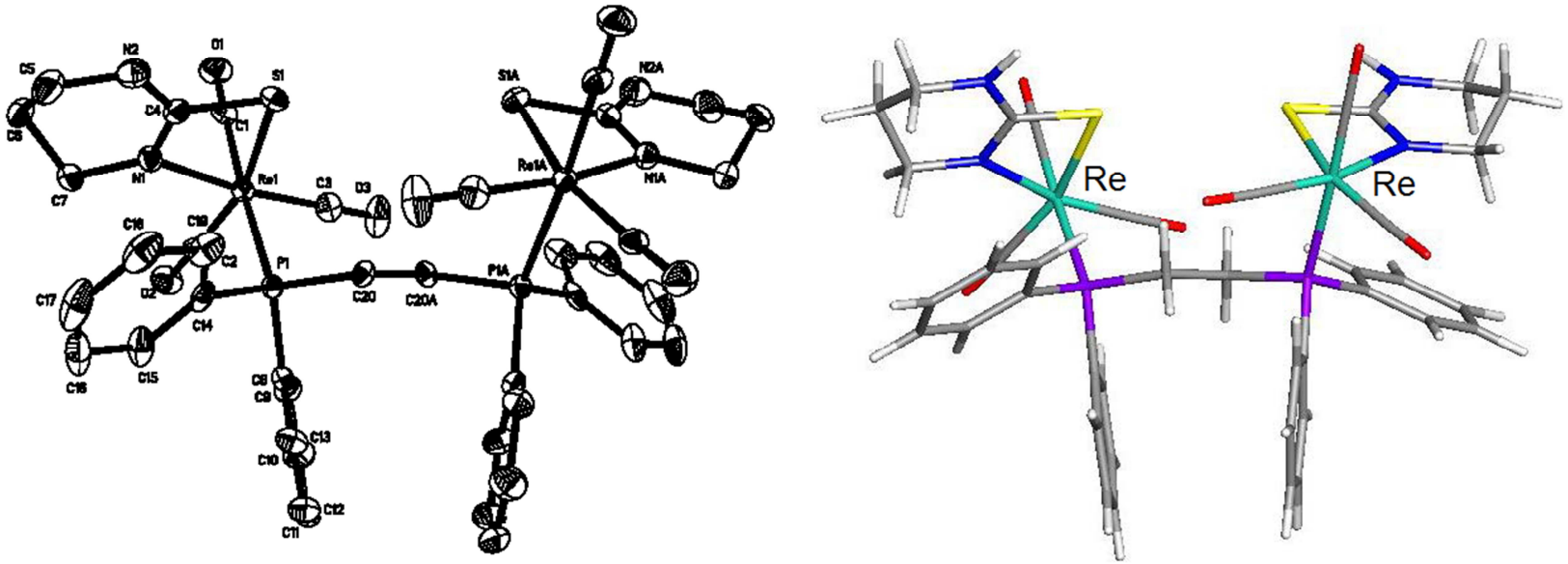

Fig. 4. Thermal ellipsoid plot of the molecular structure of **4b** (left) and the DFT-optimized structure of **J** (right). Thermal ellipsoids are displayed at 50% probability. Selected bond lengths [Å] and bond angles [°] from the X-ray diffraction structure: Re(1)–P(1) 2.4761(1), Re(1)–N(1) 2.160(4), Re(1)–S(1) 2.5450(1), P(1)–C(20) 1.845(5), C(20)–C(20A) 1.518(9), N(1)–Re(1)–S(1) 64.77(1), N(1)–Re(1)–P(1) 87.32(1), C(1)–Re(1)–S(1) 90.18(2), C(1)–Re(1)–C(2) 88.7(2).

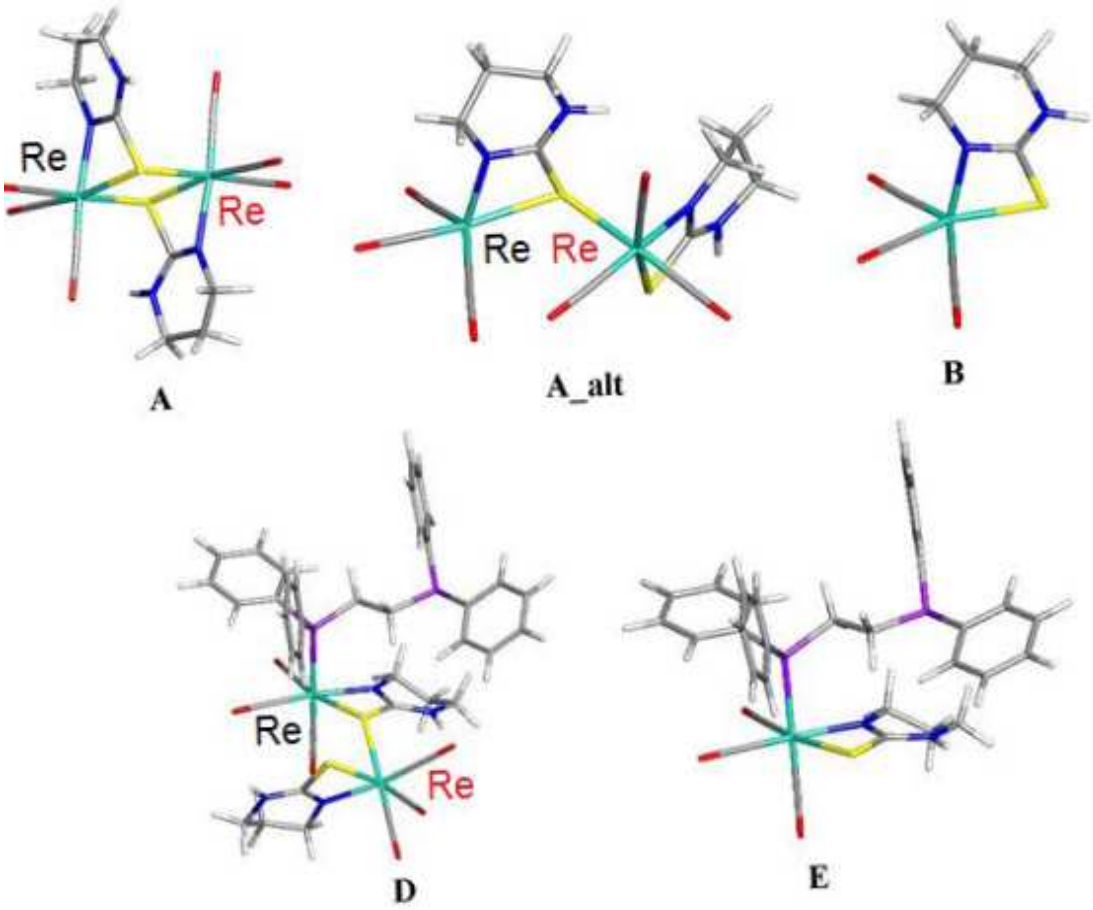

Fig. 5. DFT-optimized structures for species **A**, **A_alt**, **B**, **D**, and **E**. The optimized structure for dppe (**C**) is not shown.

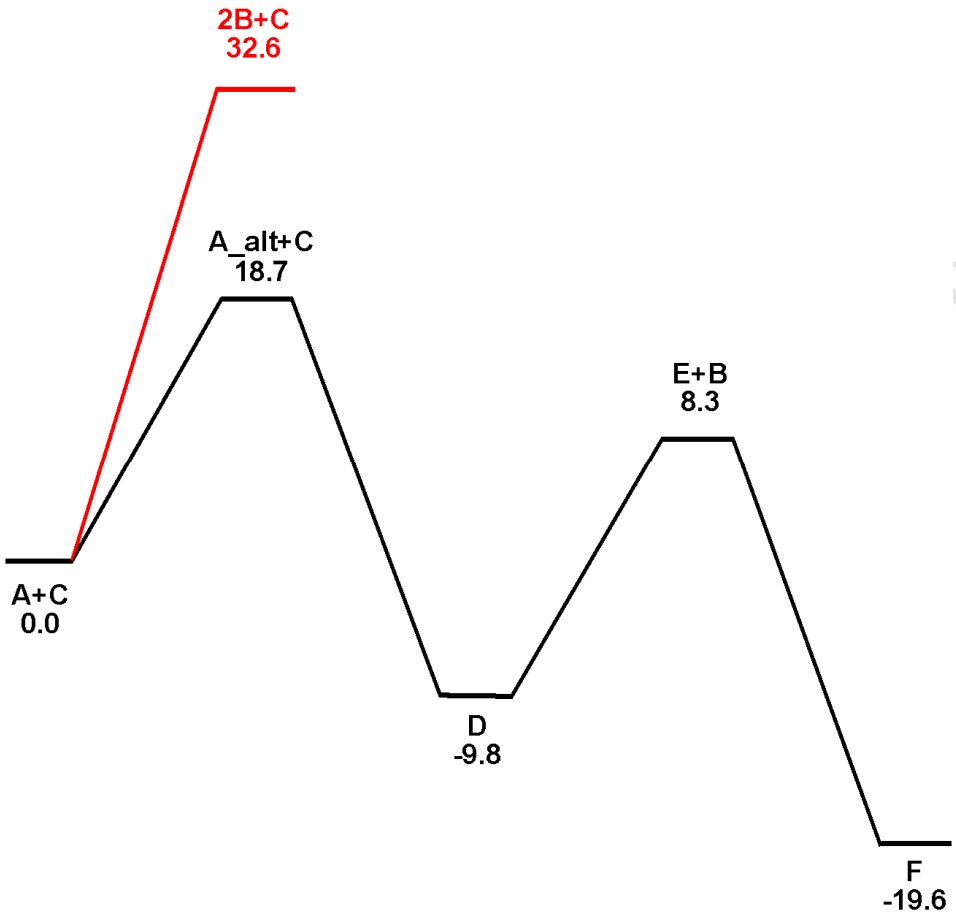

Fig. 6. Energy surface for the conversion of **A** and **C** to give **F**. The energy values for ΔH are in kcal/mol relative to **A**+**C**.

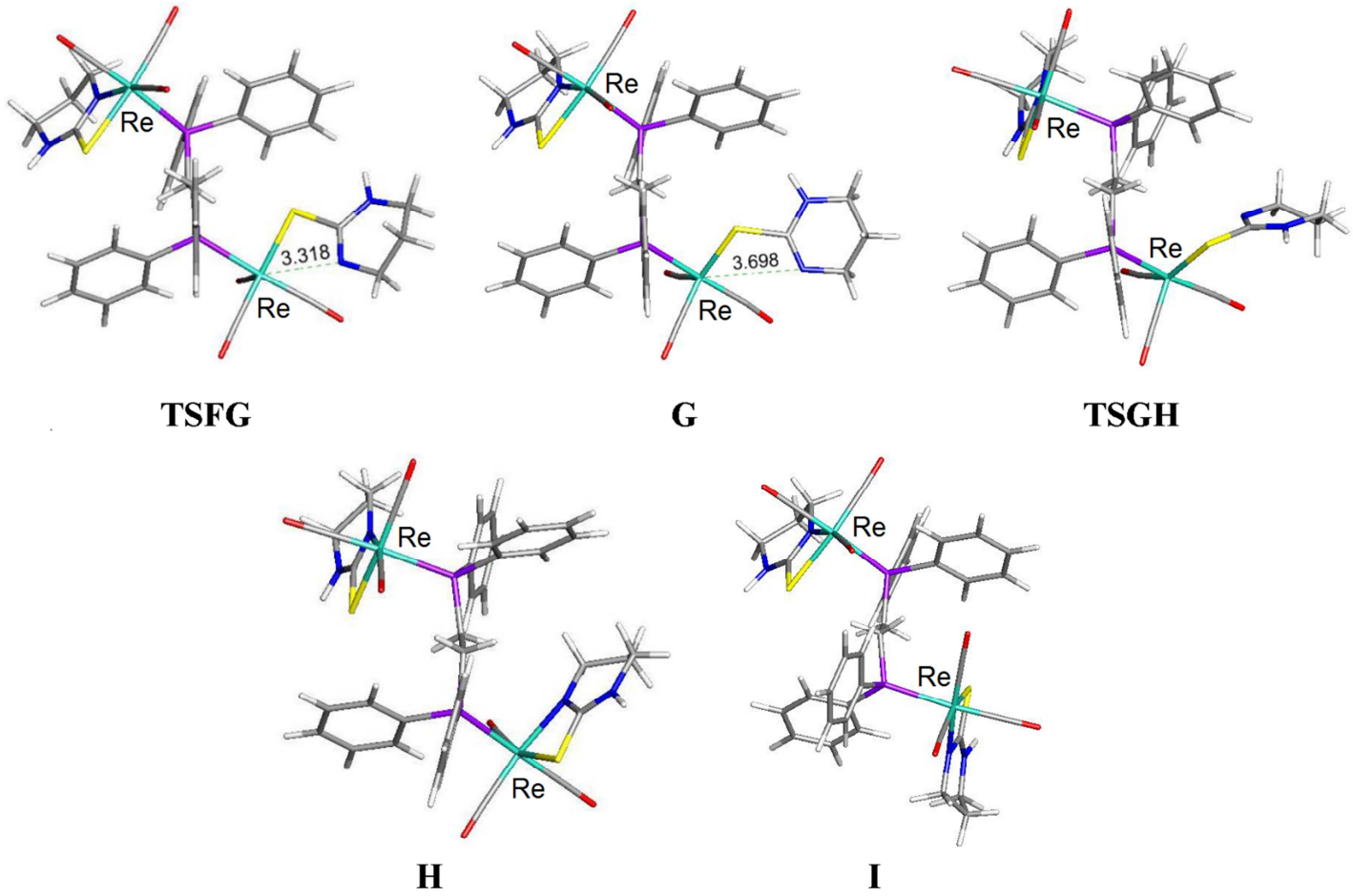

Fig. 7. DFT-optimized structures for the ground-state structures **G**, **H**, and **I**, and transition states **TSFG** and **TSGH**.

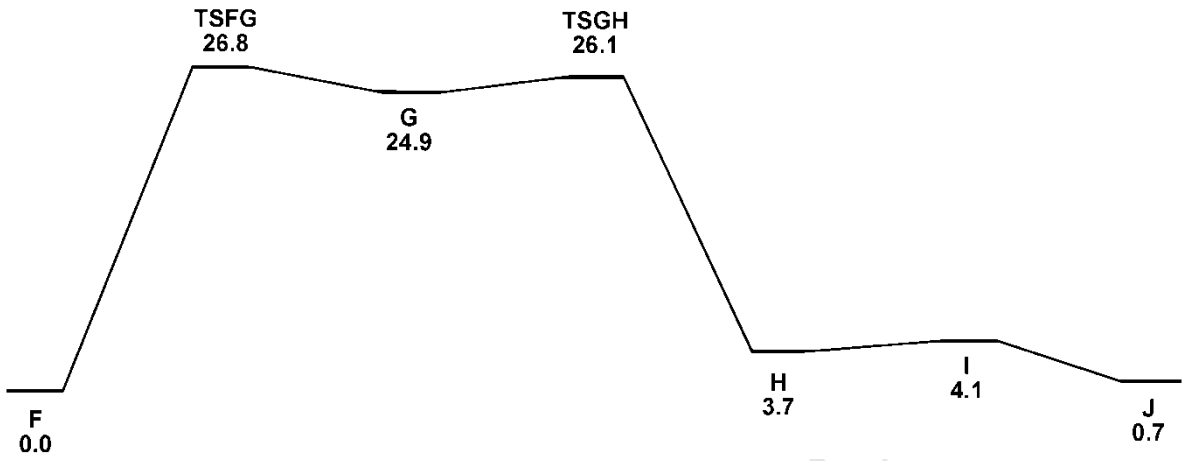

Fig. 8. Energy surface for the isomerization of **F** to give **J**. The energy values for ΔH are in kcal/mol relative to **F**.

Research Highlights

- Reactions of binuclear $[Re(CO)_3(\mu,\kappa^2\text{-S,N-thpymS})]_2$ with diphosphines
- Synthesis and structure of dppm-bridged dirhenium complex $[Re_2(CO)_4(\mu\text{-dppm})(\mu,\kappa^2\text{-S,N-thpymS})_2]$
- Structures of the two configurational isomers of $[Re(CO)_3(\kappa^2\text{-S,N-thpymS})]_2(\mu,\kappa^1,\kappa^1\text{-dppe})$